PINSTECH/NPD-121

SEGREGATION EFFECTS IN WELDED STAINLESS STEELS

J. I. AKHTER
K. A. SHOAIB
M. A. SHAIKH
M. AHMED
A. Q. MALIK

NUCLEAR PHYSICS DIVISION
Pakistan Institute of Nuclear Science and Technology
Nilore, Rawalpindi.
1987

PINSTECH/NPD-121

SEGREGATION EFFECTS IN WELDED STAINLESS STEELS

J.I. Akhter
K.A. Shoaib
M.A. Shaikh
M. Ahmed
A.Q. Malik

Nuclear Physics Division,
Pakistan Institute of Nuclear Science & Technology,
P.O. Nilore, Islamabad,

1987

CONTENTS

ABSTRACT

Welding of steels causes changes in the microstructure and chemical composition which could adversely affect the mechanical and corrosion properties. The report describes the experimental results of an investigation of segregation effects in welded austenitic stainless steels of AISI type 304, 304L, 316 and 316L using the techniques of scanning electron microscopy and electron probe microanalysis. Considerable enhancement of chromium and carbon has been observed in certain well-defined zones on the parent metal and on the weld beads. The localized change in surface composition, particularly in the parent metal, is attributed to the formation of $M_{23}C_6$ precipitates. The formation of geometrically well-defined segregation zones is explained on the basis of the time-temperature-precipitation curve of $M_{23}C_6$.

1. INTRODUCTION

There are different types of stainless steels but the main types, defined on the basis of structure, are martensitic, ferritic and austenitic steels (1). Martensitic steels contain 12-17% Cr, 0-4% Ni, 0.1-1% C and sometimes additions of Mo, V, Nb, Al and Cu. These are used in chemical and petrochemical plants, hydroelectric power generators, etc., while higher carbon steels are used for tools, bearings and cutlery. Ferritic steels consist of 15-30% Cr, low carbon but no nickel, and often contain some Mo, Nb and Ti. These steels are used in relatively mild environments, such as for kitchenware and in automobile, food and transportation industries. Austenitc stainless steels have 18-25% Cr, 8-20% Ni and low carbon. They may have some additions of Mo, Nb or Ti. There are many applications of these steels in corrosive and high temperature environments.

AISI 304 is a general-purpose corrosion-resistant austenitic stainless steel commonly used in industrial fabrication. Stainless steel of 316 type has a much higher corrosion resistance and creep strength and has specialized, but extensive, uses such as in chemical plants, as superheater piping and tube material in steam generating plants and as a structural material and a cladding alloy in conventional and advanced nuclear reactors. AISI 304L and AISI 316L are extra-low carbon versions which have improved welding properties.

Welding technique is used in the construction of modern structures. Welding involves melting and solidification of the material which could cause some changes in the microstructure and chemical composition of the material. Such changes can adversely affect the mechanical and corrosion properties. Exposure of stainless steels to higher temperatures causes their decomposition resulting in the formation of carbides and intermetallic phases. The major phases observed in type 316

stainless steel include $M_{23}C_6$, M_6C, M_7C_3 and intermetallic phases σ, χ and η with the crystal structures as FCC, FCC, HCP, tetragonal, BCC and hexagonal respectively (2,3). Formation of carbides and intermetallic phases affect the mechanical and corrosion properties of stainless steels. For example, formation of chromium carbides would result in depletion of chromium and hence in the reduction of corrosion resistance (4). The precipitation of σ phase is known to cause embrittlement in stainless steel (5).

The presence of ferrite in austenitic stainless steel plays an important role in the precipitation of carbides and intermetallic phases. Austenitic stainless steels of AISI 300 series have duplex structure, i.e., austenitic matrix has some ferrite content. Most of the steels in 300 series have ferrite contents from 5-10% at room temperature (6). Austenitic stainless steel is susceptible to hot cracking and the ferrite has beneficial effect in reducing hot cracking (7). At higher temperatures ferrite decomposes into intermetallic phases. Tavassoli et al (3) and Thomas et al (8) have investigated the decomposition of δ-ferrite and reported that $M_{23}C_6$ is the first precipitate phase to form.

Extreme segregation can take place during welding which can change the local chemistry of the material considerably. Reghunathan et al (9) reported the enhancement of Cr and Mo in the ferrite present in austenitic stainless steel. Takalo et al (10) have shown that when ferrite is present at grain boundaries it is enriched in Cr, Mo and Si. Enrichment of low melting inter-granular films with sulphur and phosphorus has also been reported (11). Using Auger electron spectroscopy it was found that phosphorus, sulphur, nitrogen, chromium and nickel segregate to the surface of 304 and 316L austenitic stainless steel (12).

The present report describes experimental results of the study of segregation effects in welded austenitic stainless steels.

2. EXPERIMENTAL

2.1 Material

The materials investigated are the austenitic steels of type AISI 304, 304L, 316 and 316L obtained from AERE Harwell and from New Laboratories, PINSTECH. Table I gives the normal compositions of these four alloys. Steels 304L and 316L have lower carbon content than 304 and 316.

2.2 Samples

The samples of steels 304, 304L and 316 were in the form of a disc of thickness 3 mm and of diameter 20 mm while the samples of steel 316L were in the form of rectangular strips, approximately 15 mm x 25 mm x 0.68 mm in size. Rectangular samples of steel 316L and 304L of the size 20mm x 20mm and thickness 3 mm were also investigated. A diametrical V-groove of 2 mm width and same depth was cut in all the 3 mm thick specimens.

2.3 Welding

The test welds were produced using tungsten inert gas welding technique with the shielding gas being argon, flowing at a rate of 5-10 lt/min. The filler metal was derived from the parent metal in the form of 1-2 mm wide strips. The tungsten electrode had a diameter of 1.0-1.6 mm. The weld travel speed ranged from 0.5-1.0 mm/sec. The welding current was about 30 A and 12 A for the circular and rectangular samples respectively. The current was reduced to 5 A and 2.5 A respectively for the circular and rectangular specimens towards the end of the welding sequence in order to account for the heat accumulation.

2.4 Etching

In order to reveal the segregated areas the samples have to be etched. During etching of the metallic specimens, dissolution of the surface proceeds at different rates for different microstructural features due to difference in chemical potential between microstructural elements. The welded samples were etched at 70 °C for 4 minutes in a 1:1 solution of conc. hydrochloric acid in water.

2.5 Microscopy

The etched samples were examined with JEOL JSM-35CF (DDS) scanning electron microscope using an electron beam of 25 KV. Microprobe analysis for most of the elements was done using automated energy dispersive system (Link 860-2). For the analysis of light elements, JEOL wavelength dispersive spectrometer DDS was used. Techniques of spot analysis, selected area analysis or line scan were used to suit particular conditions.

3. IMAGE FORMATION IN A SCANNING ELECTRON MICROSCOPE (SEM)

3.1 Interaction of Electrons with Solid

In a scanning electron microscope a beam of electrons strikes the surface of the sample under observation. If the sample is sufficiently thin, electrons may pass all the way through the sample. Some of the incident (primary) electrons are scattered in various directions when they undergo plural scattering (having one or two scattering events) or multiple scattering (having many scattering events). If the total scattering angle exceeds 90°, an electron may emerge backwards through the surface. Such electrons are termed as back-scattered electrons.

A portion of primary electrons undergo inelastic collisions and cause secondary electrons to be generated from the atoms. These secondaries move in all directions. Some of them will be directed towards the surface on which primary beam is incident. If they have sufficient energy they may be ejected out of the surface. These electrons are named secondary electrons and have a much lower energy than back-scattered electrons.

When incident electrons collide with the atoms of the specimen, most of the energy is converted to heat but some of it is used in producing X-rays and cathodoluminescence along with secondary or Auger electrons. In case of a semiconductor, irradiation with electrons will create charge carriers. By using these carriers an electromotive force image can be obtained. Fig. 1 shows various signals which can be obtained in a scanning electron microscope and also gives a schematic representation of electron beam penetration and spreading within a specimen.

3.2 Principle of SEM

In a scanning electron microscope, a narrow beam of accelerated electrons generated by a cathode passes through a set of electromagnetic lenses and is focussed onto the surface of the specimen. The diameter of the beam at the sample is very small and may be less than 0.01 μm. The beam scans the sample surface and a cathode ray tube is scanned synchronously with the electron probe. The signal from the sample in the form of the emitted secondary electrons, x-rays, etc., is fed to the grid of the cathode ray tube through a preamplifier and the image of the sample surface is formed point by point on the screen.

Secondary and back-scattered electrons, X-rays, cathodoluminescence, emf, etc., carry information about the nature of the specimen and the various images provide different information about the sample. Table II lists the information which can be obtained from various types of scanning images.

As the energy of secondary electrons is very low, only those are able to escape which originate near the surface (Fig. 1). They are thus most suitable for the observation of fine structure of the specimen surface. As the beam scans the surface, changes in composition, texture or topography at the point where the electrons strike the sample cause variation in the number of emitted secondary electrons and so image contrast is obtained.

4. ELECTRON PROBE MICROANALYSIS

The interaction of electron beam with the atoms of the sample generates characteristic X-rays in addition to continuous X-rays. By measuring the energy or wave-length of the emitted characteristic X-rays, elements present in the sample can be identified and from the intensities of the X-rays, quantitative determination can be made. There are two methods for the detection of X-rays:

1) Energy dispersive system
2) Wavelength dispersive system

4.1 Energy Dispersive System (EDS)

A semiconductor Si(Li) detector is used for X-ray detection. X-rays produce free charge carriers which are collected under the influence of a voltage bias. The number of these carriers is proportional to the energy of the X-ray being absorbed. The voltage pulse from the preamplifier is amplified and fed into the multichannel

analyser and so various characteristic X-rays can be analysed. In this method rapid analysis can be done as signal detection is simultaneous for all X-rays. However, elements lighter than sodium can not be detected due to absorption of X-rays in the thin beryllium window placed in front of the detector.

4.2 Wavelength Dispersive System (WDS)

In this system the emitted X-rays falling on an analysing crystal will be diffracted by the crystal only if they satisfy Bragg's Law:

$$n\lambda = 2d \sin\theta,$$

where n is the order of diffraction,
λ is the wavelength of X-rays,
d is the interplanar spacing of the crystal and
θ is the Bragg angle.

Wavelength dispersion by the spectrometer crystal enables the detection of an element.

A proportional counter is used for the detection of the X-rays. The signal is fed into a preamplifier, amplifier and then to pulse height analyser. Only one wavelength is detected at one time, but the spectra can be recorded by scanning the spectrometer slowly across a range of wavelengths.

WDS is capable of detecting elements down to boron and even to beryllium with special crystals. Resolution of WDS is much better than that of EDS, approximately 20eV compared to 150 eV for EDS. Also peak-to-background ratio is much higher for WDS than that for EDS. However, analysis with WDS takes a very long time.

5. RESULTS

Visual inspection of the etched samples showed large black segregated zones, nearly 1 mm in width, in some parts of the parent metal in all the samples of stainless steels. These zones, for the disc and rectangular specimens, are illustrated at low magnification in the micrograph, Fig. 2. The outstanding feature of these zones was their geometry. In circular specimens the zones were towards the end of the welding sequence and were a circular segment around the last bead, whereas in the rectangular specimens the zone was a straight line parallel to the welded zone which grew darker towards the end of the welding sequence. Low magnification examination in an optical stereomicroscope also showed scattered dark segregated spots on the weld metal beads, their density generally increasing towards the last bead.

The results can be discussed in terms of Cr/Fe and Ni/Fe ratios in various areas of the specimens. X-ray microanalysis measurements have been made at particular spots, as well as in the selected areas, representing (a) the heat affected zones; (b) the weld beads (both the first and the last); (c) overlapping boundaries of two beads; and (d) the parent metal. The results show that average composition of the heat affected zones and of the welding beads was generally the same as that in the parent metal. However, in isolated spots considerable increase was observed in the Cr content. In the heat affected zones these spots are seen near the segregated matrix areas while the density of such spots on weld beads increases towards the last bead. Occasional spots were also found to be enriched in Ni and, in case of 316 and 316L steels, also in Mo. The results are summarized in Table III in terms of Cr/Fe and Ni/Fe ratios for the parent metal and for the selected spots with high segregation in the welded specimens.

The parent matrix in all the four steels exhibited marked enhancement of Cr in the segregation zones, the maximum value being 59% in 304 steel. Fig.3 is a micrograph of such a highly segregated area in 304 steel and shows the line profiles of Cr and Fe with the line scan done along the central straight line. A weld bead is shown at the right corner and the segregates on parent metal can be seen to be in the form of thin flakes. It is evident that Cr is increased considerably in the segregated zone while Fe is decreased. Similar effect can also be seen in a narrow region of the heat affected zone adjacent to the weld bead. The superficial nature of the zones is revealed in Fig. 4 which gives the Cr/Fe and Ni/Fe ratios and the carbon profile along the common line in a selected area within the weld beads of 304 sample cut in cross-section. It can be seen that the depth of the segregated area is about 20 μm.

For other steel samples similar results are obtained for the segregated areas on the parent metal. However, the magnitude of Cr/Fe ratio differs in all the samples. For 316 and 316L steels an increase in Ni/Fe ratio, accompanied by increase in Mo, has also been observed in such segregated areas. Enhancement of chromium in the segregated area would lead to its depletion in the areas of sample in the vicinity. Simple calculations show that, if the additional chromium in the segregated zone is assumed to come from the volume of the sample underneath this zone, it would result in a reduction of 0.5% in the chromium content. This is within the experimental error and is the likely reason why the depletion could not be detected.

An increase in Cr/Fe ratio is often observed at the overlapping of two beads. This increase is prominent in the case of 316L steel where segregation is observed over a wider area. A micrograph of the microscopic zones of high segregation in such an area, together with the trace of Cr/Fe and Ni/Fe ratios, is shown in Fig. 5. The line scan is done along the central straight line on the micrograph. The increase in Cr/Fe ratio is obvious in the segregated zone while at some points in these areas high Ni/Fe ratio plus increase in Mo content is also observed.

Carbon content of the segregated areas is an important clue in the determination of the nature of the segregates. Analysis for carbon at various spots on the segregated zones revealed an increase upto eight times the value in the parent metal.

6. DISCUSSION

The observed microstructural segregation in the four steels can be discussed on the basis of the phase diagram of the iron-chromium-nickel system. Although the steels investigated are austenitic, the small amount of δ-ferrite formed during solidification of welds is known to cause local changes in composition. It has been conclusively reported (9,11,13,14) that the ferrite phase is enriched in Cr, Mo and Si while an enhancement of Ni occurs in the austenite.

Extreme segregation of Cr has been observed in aged or heat-treated specimens. In many austenitic welds the ferrite transforms to the Cr-rich sigma phase during high temperature (650°C) service and is the source of internal cracking (15,16). The Cr-Fe sigma phase contains 42-48% Cr, as can be seen from the Cr-Fe phase diagram (Fig. 6) (17) but its formula can vastly vary depending upon exact composition of the alloy. The amount of Cr in some of the segregated areas is very high leading to a suspicion of sigma phase. However, the presence of this phase is ruled out in the present case as its formation requires long ageing time at high temperature (3,18,19) and its growth is prohibited by the presence of Ni (19,20).

Since the shield gas used was commercial grade argon which might contain small amounts of oxygen, the formation of chromium oxide cannot be ruled out. In fact Auger electron spectroscopy of the segregated areas had shown an enhancement of oxygen, in addition to that of C and Cr, at some spots. However, this increase in oxygen content was not as widespread as that of carbon as is noted in the earlier section.

The segregation of Cr in the form of oxide is further not corroborated during experiments conducted on rod shaped specimens whose one end is heated to molten state and analysis of segregation is done on the interior of slices cut at various distances from the molten zone (21). The observation of very distinct segregation of Cr in these specimens indicates that this is not in the form of oxides since oxygen is not available in the interior of the rod.

The observed segregation effect, particularly on the parent metal, may be attributed to the precipitation of $M_{23}C_6$ which is a Cr-rich carbide with a complex f.c.c. structure. Its identification is confirmed by the enhancement of both Cr and C in the segregated area (22). The nucleation and growth of this carbide is rapid below about 900°C due to the fast diffusion of both Cr and interstitial C rejected from the austenitic matrix. Varying amounts of other atoms, such as Fe, Ni and Mo, can replace Cr in the lattice of $M_{23}C_6$ (19) accounting for the observed presence of these elements in the segregated areas.

The formation of well-defined zones of segregation could be explained on the basis of time-temperature-precipitation curve (2) for $M_{23}C_6$ which is shown in Fig. 7 for 316 steel. Such diagrams are modified by composition and thermo-mechanical pre-treatment and could be displaced in terms of time-temperature coordinates but they essentially retain the same features. Thus the TTP curves of steels studied in the present work are likely to be similar. It is seen from Fig. 7 that $M_{23}C_6$ is by far the earliest phase to precipitate as compared to the intermetallic phases η , χ and σ . Moreover, the nose of the curve for $M_{23}C_6$ indicates the temperature at which the growth of carbides is most rapid.

In both the circular and rectangular specimens the segregated zone appears near the end of welding sequence. From the TTP curve it is clear that precipitation of $M_{23}C_6$ results if the sample remains at a particular temperature for a certain

period of time. Though temperature at other points may be high enough for precipitation, yet time is not sufficient. The area near the end of welding sequence is expected to fulfill the requirements of both time and temperature. The occurrence of segregated zone in the form of a circular segment in circular samples and a line parallel to beads in rectangular samples is expected due to difference in the shape of isotherms on account of sample geometry.

REFERENCES

1. F.B. Pickering, Int. Metals Rev. Review 211, 227 (1976).
2. B. Weiss and R. Stickler, Metall Trans. 3, 851 (1972).
3. A.A. Tavassoli, A. Bisson and P. Soulat, Metal Sci. 18, 345 (1984).
4. A. Boeuf, R. Coppola, P. Zambondi, et al. J. Mater. Sci. 16, 1975 (1981).
5. Y. Maehara, Y. Ohmori, J. Murayama, N. Fujino and T. Kunitake, Metal Sci. 17, 541 (1983).
6. N. Suutala, T. Takalo and T. Moisio, Metall. Trans. A, 11A, 717 (1980).
7. T. Ogawa and E. Tsunetomi, Welding J. 61, 82S (1982).
8. R.G. Thomas, R.D. Nicholson and R.A. Farrar, Metals Technol. 11, 61 (1984).
9. V.S. Ragunathan, V. Seetharaman, S. Venkadesan and P. Rodriguez, Metall. Trans. 10A, 1683 (1979).
10. T. Takalo, N. Suutala and T. Moisio, Metall. Trans. 10A, 1173 (1979).
11. J.C. Lippold and W.F. Savage, Welding J. 61, 388S (1982).
12. C.L. Briant and R.A. Mulford, Metall. Trans. 13A, 745 (1982).
13. G.L. Leone and H.W. Kerr, Welding J, 61, 13S (1982).
14. J.A. Brooks, A.J. West and A.W. Thompson, Metall. Trans 14A, 75 (1983).
15. F.R. Beckitt, J. Iron Steel Inst. 207, 632 (1969).
16. J.O. Stiegler, R.T. King and G.M. Goodwin, J. Eng. Mater. Technol. 97, 245 (1975).
17. M. Hansen and K. Anderko, "Constitution of binary alloys" McGraw-Hill, New York; Springer, Berlin (1958), p.527.
18. E.O. Hall and J.H. Algie, Metall. Rev. 11, 61 (1966).
19. D.V. Edmonds and R.W. Honeycombe, "Precipitation Processes in Solids" Ed. K.C. Russel and H.I. Aaronson. The Metallurgical Soc. of AIME (1978), p.121.
20. J.M. Leitnaker, Welding J. 61, 9S (1982).
21. A. Waheed, Private communication.
22. J.K.L. Lai, D.J. Chastell and P.E.J. Flewitt, Mater. Sci. Eng. 49, 19 (1981).

Table I: Composition of the investigated stainless steels (wt%)

Sample	Fe	Cr	Ni	Mn	Mo	C	N	Si	P	S
304	67.91	19.0	9.3	2.0	-	0.08	0.03	1.00	0.0045	0.03
304L	68.56	19.0	10.0	2.0	-	0.03	0.03	1.00	0.0045	0.03
316	66.18	17.6	11.6	1.32	2.7	0.06	0.03	0.51	0.0015	0.002
316L	65.41	17.0	12.0	2.00	2.5	0.03	0.03	1.00	0.0045	0.03

Table II: Major information obtainable from various scanning images.

Type of Scanning Image	Major Information
Secondary electron	Surface structure, magnetic domains, potential distribution
Backscattered electron	Composition, topography, crystalline state
Transmitted electron	Transmission image, composition, crystalline state
Auger electron	Elemental distribution of surface
Cathodoluminescence	Visible or infrared luminescence
X-ray	Elemental distribution
Electromotive force	Electromotive force distribution in semiconductor devices

Table III: Cr/Fe ratio, and Ni/Fe ratio (in brackets), for the steels investigated. The values, other than those for parent metal, represent only those spots or areas with high segregation.

Sample	Parent Metal (average)	Weld First Bead	Weld Last Bead	Heat Affected Zone	Overlapping Bounderies of Beads	Base Metal Segregation
304	0.28(0.16)	1.22(0.16)	1.37(0.35)	1.69(0.31)	1.55(0.33)	1.96(0.30)
304L	0.28(0.11)	0.32(0.11)	0.33(0.11)	0.44(0.11)	0.34(0.11)	1.22(0.17)
316	0.27(0.19)	0.28(0.18)	0.29(0.19)	0.35(0.24)	0.59(0.13)	0.65(0.38)
316L	0.26(0.18)	0.32(0.18)	1.52(0.34)	0.79(0.33)	2.11(0.49)	0.93(0.49)

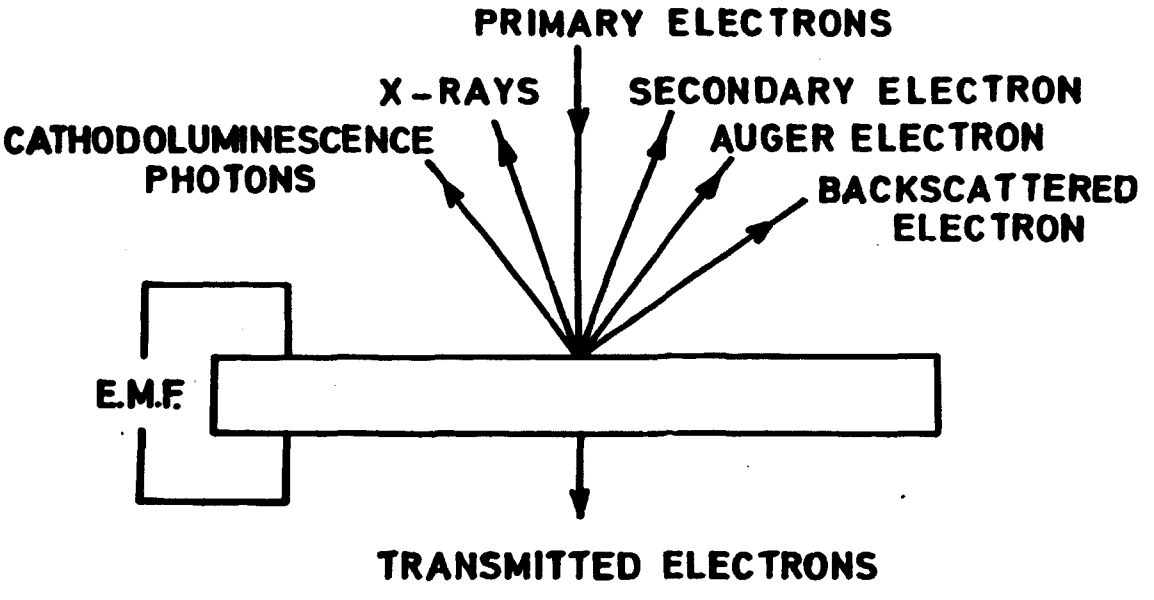

(a)

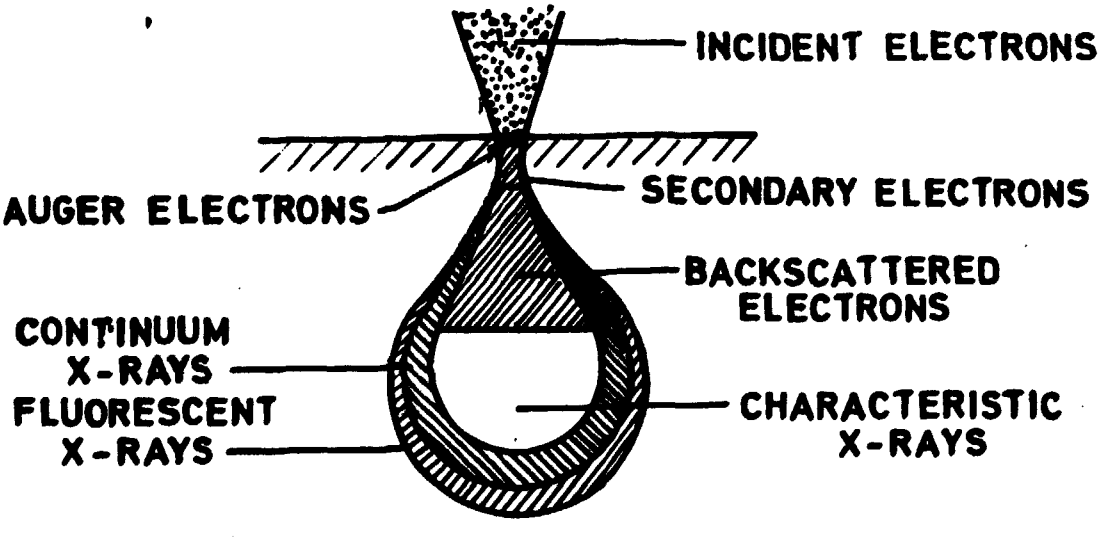

(b)

Fig. 1. (a) SIGNALS OBTAINED FROM A SCANNING ELECTRON MICROSCOPE

Fig. 1. (b) SCHEMATIC REPRESENTATION OF ELECTRON BEAM PENETRATION AND SPREADING WITH IN A SAMPLE.

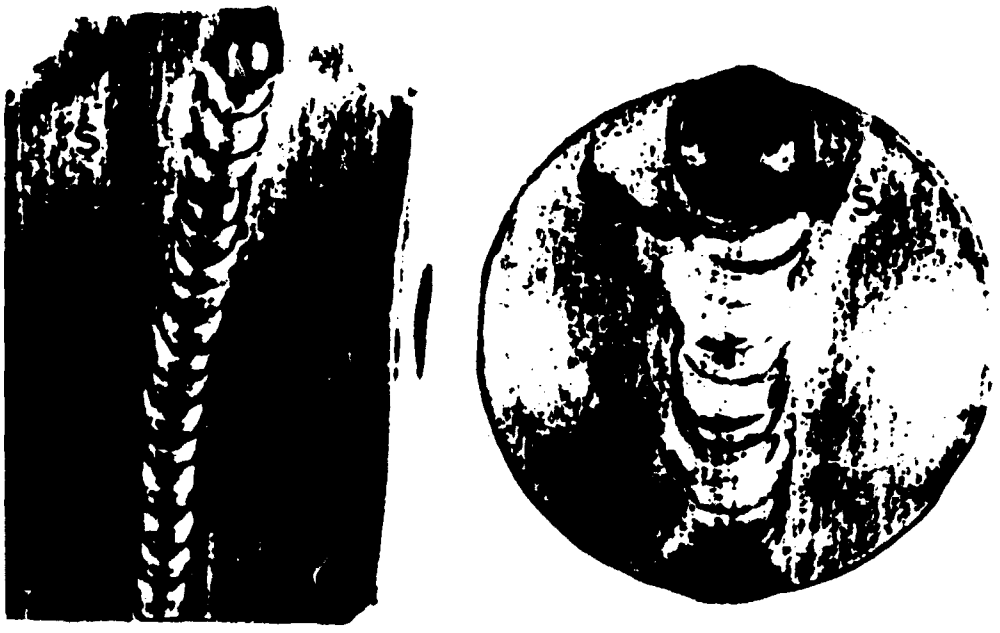

Fig.2. Low magnification photograph of welded areas and segregated zones (S).

Fig. 3. Segregated area on the parent metal in welded 304 steel.

Fig. 4. Cr / Fe, Ni / Fe and carbon profiles in cross-sectional slice across the weld.

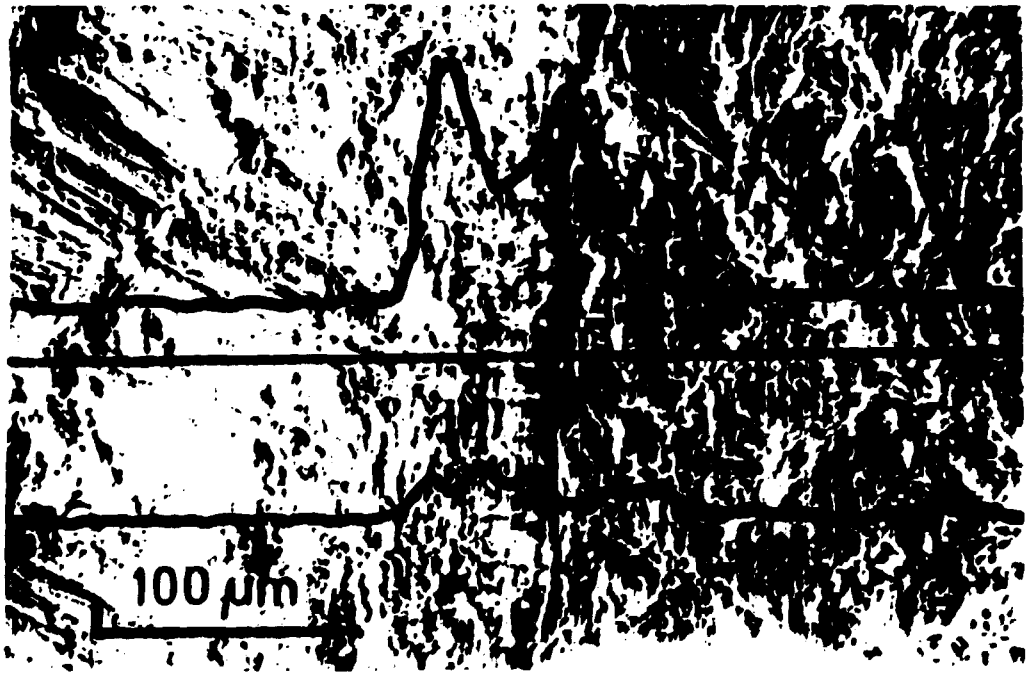

Fig. 5. Segregated zone along the overlapping boundary of two weld beads together with the profiles of Cr / Fe and Ni / Fe.

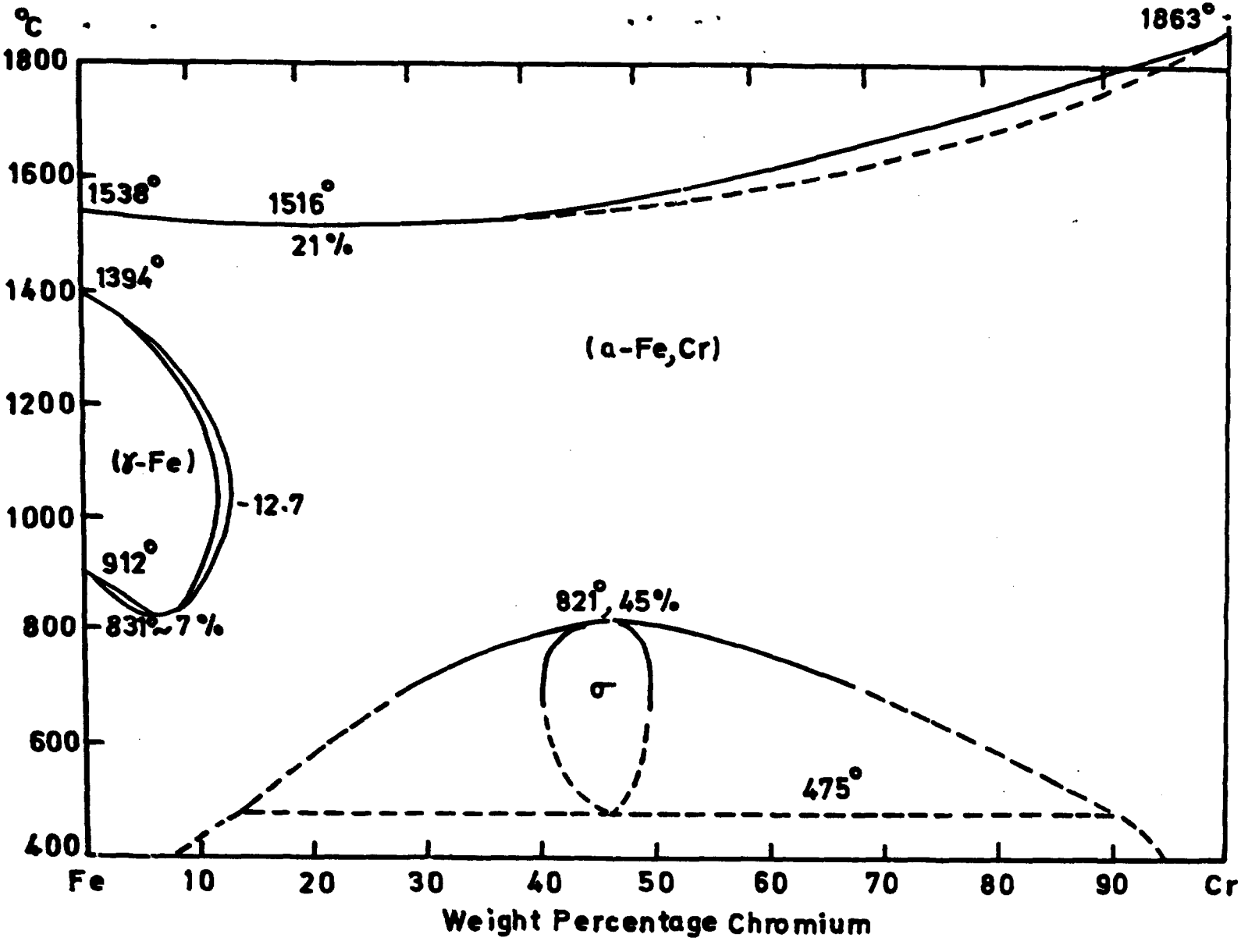

Fig. 6. Iron-chromium equilibrium diagram showing composition of sigma phase.

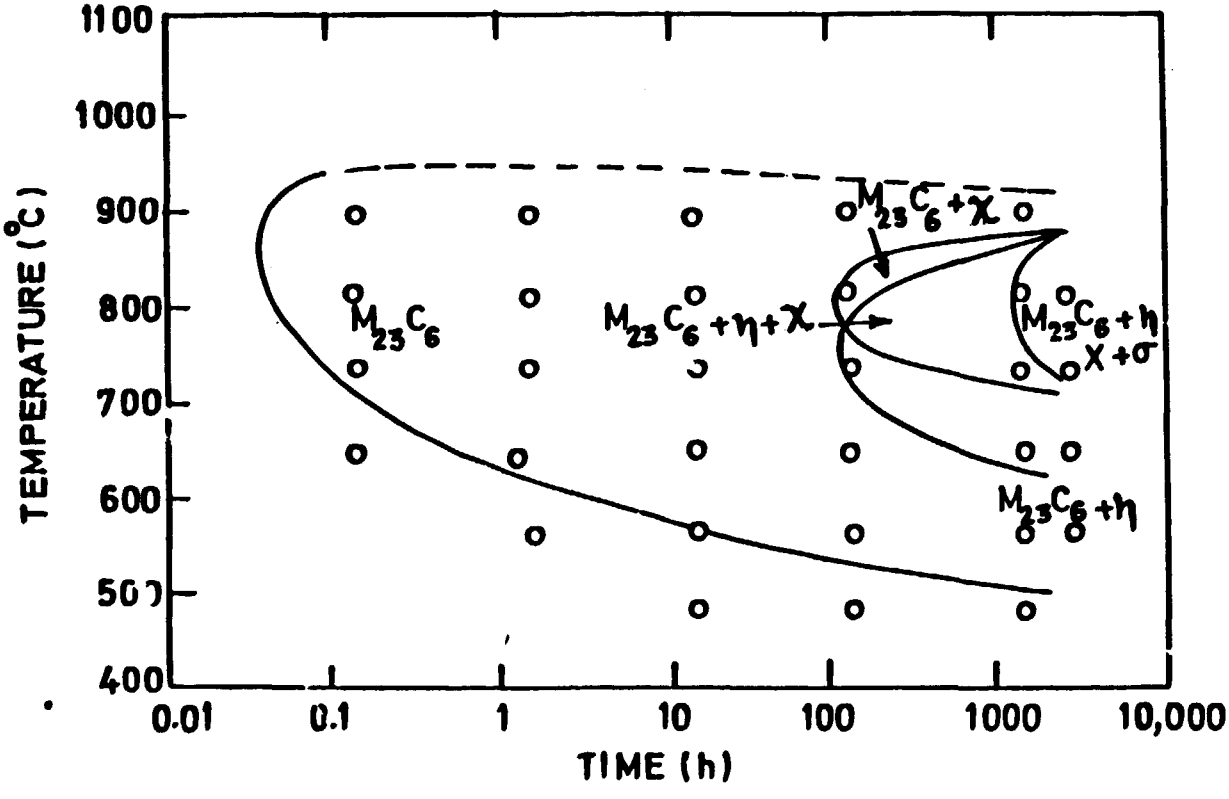

Fig. 7. Time-temperature-precipitation curve for stainless steel of type AISI 316 (from ref. 2).

Printing Corporation of Pakistan Press, Islamabad